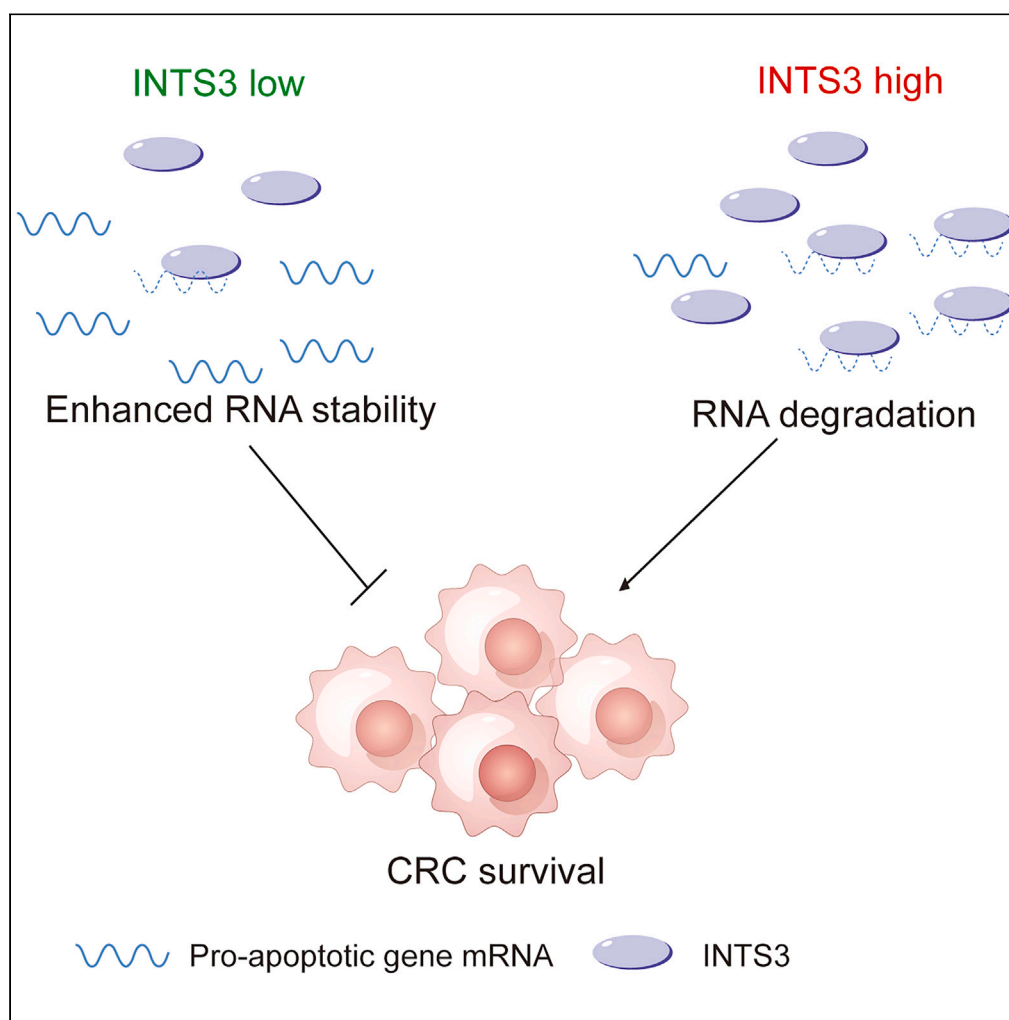


Article

CRISPR-Cas9 screening identifies INTS3 as an anti-apoptotic RNA-binding protein and therapeutic target for colorectal cancer



Zhiwei Wang,
Cheng Zhang, Jing
Guo, ..., Zhenzhen
Chen, Pingping
Zhu, Qiankun He

zhup@zzu.edu.cn (P.Z.)
qiankunhe@zzu.edu.cn (Q.H.)

Highlights

CRISPR screen identifies 27
potential RBPs with role in
supporting CRC survival

INTS3 destabilizes pro-
apoptotic gene transcripts
and contributes to CRC
survival

DOTAP/cholesterol-
mshINTS3 nanoparticles
inhibits CRC tumor growth

Wang et al., iScience 27,
109676
May 17, 2024 © 2024 The
Authors. Published by Elsevier
Inc.
[https://doi.org/10.1016/
j.isci.2024.109676](https://doi.org/10.1016/j.isci.2024.109676)

Article

CRISPR-Cas9 screening identifies INTS3 as an anti-apoptotic RNA-binding protein and therapeutic target for colorectal cancer

Zhiwei Wang,¹ Cheng Zhang,¹ Jing Guo,¹ Yanmei Yang,² Peixian Li,¹ Ziyang Wang,¹ Sijia Liu,¹ Lulu Zhang,¹ Xiaoyu Zeng,¹ Jincheng Zhai,¹ Xinyong Wang,¹ Qi Zhao,³ Zhenzhen Chen,¹ Pingping Zhu,^{1,*} and Qiankun He^{1,4,*}

SUMMARY

Growing evidences indicate that RNA-binding proteins (RBPs) play critical roles in regulating the RNA splicing, polyadenylation, stability, localization, translation, and turnover. Abnormal expression of RBPs can promote tumorigenesis. Here, we performed a CRISPR screen using an RBP pooled CRISPR knockout library and identified 27 potential RBPs with role in supporting colorectal cancer (CRC) survival. We found that the deletion/depletion of INTS3 triggered apoptosis in CRC. The *in vitro* experiments and RNA sequencing revealed that INTS3 destabilized pro-apoptotic gene transcripts and contributed to the survival of CRC cells. INTS3 loss delayed CRC cells growth *in vivo*. Furthermore, delivery of DOTAP/cholesterol-mshINTS3 nanoparticles inhibited CRC tumor growth. Collectively, our work highlights the role of INTS3 in supporting CRC survival and provides several novel therapeutic targets for treatment.

INTRODUCTION

Colorectal cancer (CRC) is one of leading cancer types with high morbidity and mortality.¹ Moreover, the CRC mortality among young adults has continued to increase in the past 15 years.² Despite improvements in surgical resection, adjuvant chemotherapy, and targeted treatment, many CRC patients still suffer from unresectable tumors, tumor recurrence or metastasis.^{3–5} Therefore, there is an urgent need to identify driver genes and therapeutically relevant targets of CRC.

Biological information transfer from DNA to RNA then protein ("Central Dogma" proposed by Crick), and thus DNA-binding proteins (DBPs, also termed as transcription factors) and RNA-binding proteins (RBPs) pivotally control gene expression signatures to modulate cellular homeostasis, serving as key regulators of cell growth and survival.⁶ Most recently, some nuclear-located RBPs have also been identified as transcription modulators via chromatin-associated RNAs, such as RBM25⁷ and YTHDC1.⁸ Tumor cells often upregulate post-transcriptional processing regulated by RBPs to meet the high demands of various biological processes, such as proliferation, anti-apoptosis, and metastasis. Generally, RBPs regulate RNA splicing, polyadenylation, localization, translation, and turnover and RBP-mediated post-transcriptional processes may play an oncogenic role in cancers.^{9,10} A large number of DBPs (transcription factors) have been identified and well characterized in CRC, but aberrant RBP regulation that contributes to tumor progression is poorly understood. Recently, we characterized several functional RBPs in cancer cells, including insulin-like growth factor 2 mRNA binding protein (IGF2BP2) and K-homology splicing regulatory protein (KSRP). IGF2BP2 associates with N-methyladenosine (m6A)-modified *E2F6/E2F3* mRNAs to inhibit mRNA decay, and thus drives the self-renewal of liver tumor initiating cells.¹¹ KSRP binds to the 3'-UTR of *HOXC10* mRNA to induce *HOXC10* decay, and *HOXC10* in turn promotes the self-renewal of CRC self-renewal via FZD3-Wnt signaling.¹² However, our research upon these individual RBPs cannot give an overall understanding of RBPs in CRC.

CRISPR screening is an efficient method to identify functional genes in cancer. The CRISPR platform enables high-throughput interrogation of genes with reduced off-target effects and stronger genetic editing capability. In recent years, the development of CRISPR techniques has resulted in increasing complexity and compatibility.¹³ Given the complicated mechanism of tumorigenesis, CRISPR-Cas9 screening is a reliable and high-throughput strategy to explore the key regulator genes for cancer cell survival, growth, drug resistance, and immune resistance.¹⁴ Therefore, CRISPR-Cas9 screening is a useful tool for identifying target genes for drug discovery and gene therapy, and RBP CRISPR screening in CRC cells has not been reported to our knowledge.

Here, we used an RBP pooled CRISPR knockout library to comprehensively study critical RBPs for CRC propagation and survival. In this screening, 27 RBPs required for CRC propagation and survival were identified. Network analysis showed that these genes were involved in tRNA aminoacylation for protein translation, mRNA splicing, ncRNA processing and translation. Notably, we identified that INTS3 was

¹School of Life Sciences, Zhengzhou University, 100 Kexue Road, Zhengzhou 450001, China

²Research Center of Basic Medicine, Academy of Medical Sciences, Zhengzhou University, Zhengzhou 450001, China

³Department of oncology, The First Affiliated Hospital of Zhengzhou University, Zhengzhou 450052, China

⁴Lead contact

*Correspondence: zhup@zzu.edu.cn (P.Z.), qiankunhe@zzu.edu.cn (Q.H.)

<https://doi.org/10.1016/j.isci.2024.109676>



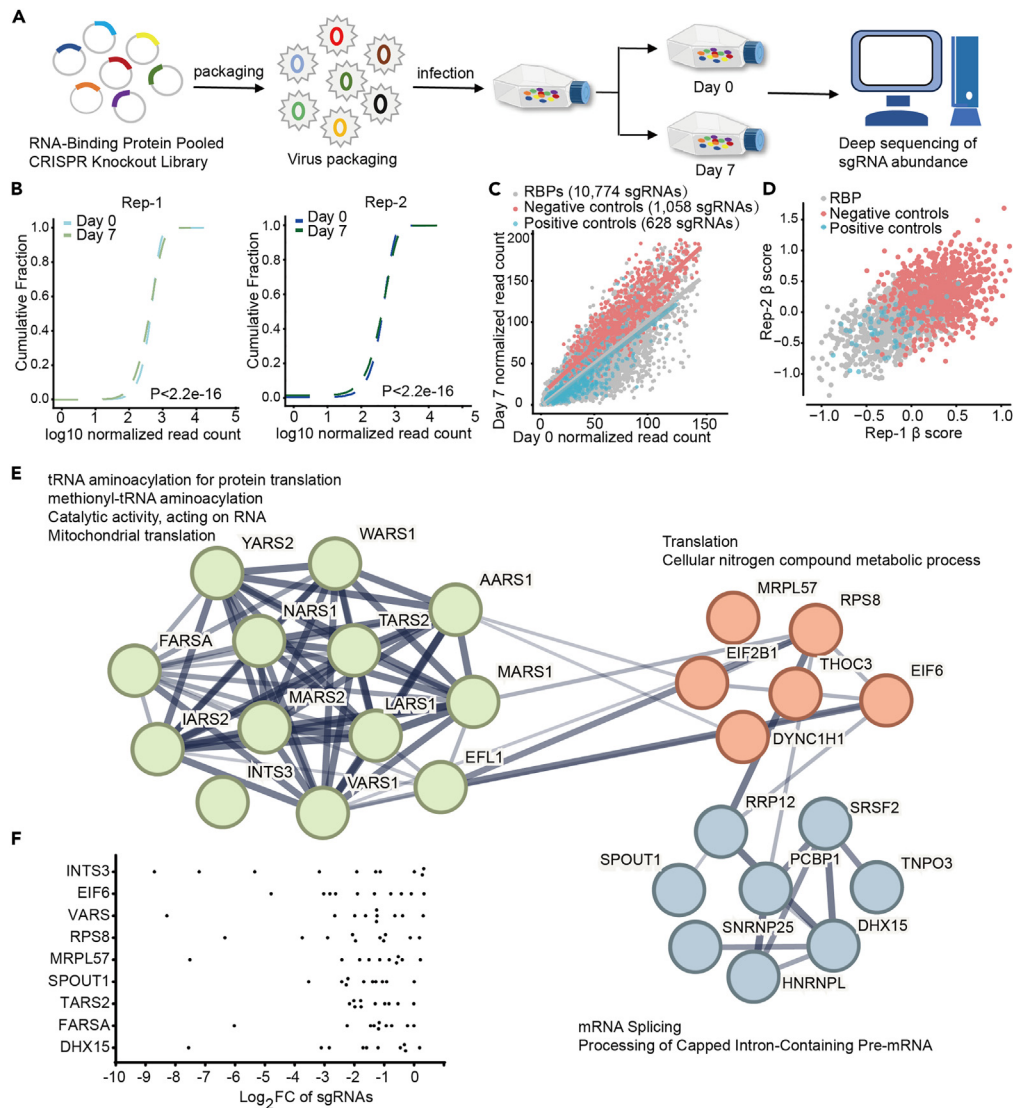


Figure 1. CRISPR-Cas9 screening of RBPs in CRC cells

- (A) Pipeline of RBP pooled CRISPR knockout library propagation/survival screening in CRC cell line.
 (B) Cumulative distribution of normalized read counts for sgRNAs in each replicate. Two-sided Kolmogorov-Smirnov tests compared with day 0.
 (C) Scatterplot displaying normalized read counts on day 7 compared with day 0. Genes are categorized by negative control, positive control and RBP.
 (D) Comparison of β score replicates on day 7.
 (E) STRING protein-protein interaction (PPI) network of 27 critical RBP candidates.
 (F) The distribution of \log_2 -fold change (FC) of sgRNAs of the top nine depleted RBPs.

overexpressed in CRC patients and correlated to poor clinical outcomes. Meanwhile, INTS3 depletion/deletion inhibited CRC growth *in vitro* and *in vivo*. Through RNA-decay sequencing, we found that INTS3 reduced the expression of pro-apoptotic genes TXNIP, CLU and NR4A1, by impairing the stability of these mRNAs, thereby enhancing CRC survival. Therefore, our data demonstrated that loss of INTS3 was negatively associated with CRC survival, indicating that INTS3 is an oncogenic RBP in CRC and serving as a promising target for CRC treatment.

RESULTS

CRISPR-Cas9 screening of RBPs in CRC cells

In order to identify critical RBPs in CRC, we performed a CRISPR-Cas9 screening using an RBP pooled CRISPR knockout library targeting 1,078 RBPs.¹⁵ The library was packaged to infect SW620 cells. After puromycin selection, single guide RNA (sgRNA)-transduced SW620 cells were collected and extracted for genomic DNA on day 7 (Figure 1A). sgRNAs sequencing analysis showed a high correlation between the two

replications on day 0 and day 7 (Figure S1A). After 7 days propagation, the distributions of sgRNA counts were significantly different compared to day 0 cells, and a significant reduction in sgRNA diversity was observed in surviving cells on day 7 (Figures 1B and S1B). Comparing with negative control sgRNAs, positive control sgRNAs were strongly deleted (Figures 1C and 1D). These data demonstrated the validity and reliability of propagation/survival-dependent RBP screening in CRC cells. Integrating two replications, we identified 27 critical RBP candidates in CRC propagation and survival. STRING analysis further indicated candidate genes were clustered into three pathways: tRNA aminoacylation for protein translation and mitochondrial translation, mRNA splicing and translation (Figure 1E). Several RBP candidates which have been identified as oncogenes in CRC were identified and ranked high in our screening, including EIF6,¹⁶ FARSA,¹⁷ RRP12¹⁸ and EFL1¹⁹ (Figure 1E). Then, we explored The Cancer Genome Atlas (TCGA) database and analyzed by The University of Alabama at Birmingham CANcer data analysis Portal (UALCAN) data analysis portal and found that 85% of RBP candidates are highly expressed in CRC tumors (Figure S1C). We then determined a functional RBP for further investigation. As shown in Figure 1F, sgRNAs of INTS3 were most significantly depleted after 7 days' culture and ranked the first in our screening results, indicating that INTS3 was a potential oncogenic RBP. Moreover, the function of INTS3 in CRC cells is poorly explored, and thus we focused on INTS3 in this work.

INTS3 is highly expressed in CRC and related to clinical severity

To better determine the potential oncogenic role of INTS3 in CRC, we firstly performed a multi-tumor omics analysis using UALCAN and Tumor Immune Estimation Resource (TIMER) databases to detect *INTS3* mRNA expression in various cancer types, and found that *INTS3* expression is generally increased in many tumors (Figures 2A and S2). Then, we analyzed *INTS3* expression in CRC tumor tissues with multiple databases such as Encyclopedia of RNA Interactomes (ENCORI), Gene Expression Profiling Interactive Analysis 2 (GEPIA2) and differential gene expression analysis in Tumor, Normal, and Metastatic tissues (TNMplot). Consistent with the results of multi-tumor omics analysis, the expression levels of *INTS3* in CRC tissues were relatively higher than that in normal tissues (Figures 2B–2D). Furthermore, metastatic CRC tissues showed higher *INTS3* expression levels than primary CRC tissues according to TNMplot database (Figure 2D). The Clinical Proteomic Tumor Analysis Consortium (CPTAC) database also demonstrated that CRC tissues had higher levels of *INTS3* protein (Figure 2E). TCGA database revealed that high *INTS3* expression was significantly correlated with poor survival of CRC patients (Figure 2F). To verify the expression level of *INTS3* in CRC cell lines and clinical tissues, we performed RT-qPCR and western blot assays. Comparing to human normal colonic epithelial cell NCM460, *INTS3* is overexpressed in CRC cell lines, including RKO, HCT116, LOVO, HT29, and SW620 (Figure 2G). *INTS3* protein was also higher expressed in CRC tissues than that in normal adjacent counterpart (Figures 2H and 2I). Altogether, *INTS3* was overexpressed in CRC and its expression was correlated with CRC metastasis and clinical severity.

INTS3 is required for CRC cell survival via apoptosis inhibition

To validate the function of *INTS3*, *INTS3* knockout SW620 CRC cell lines were generated through CRISPR-Cas9 approach and we also performed *INTS3* knockdown in SW620, HCT116, and RKO CRC cell lines. The knockout/knockdown efficiency was confirmed by western blot (Figure S3A). Taking advantage of these *INTS3* LOF cells, we first performed propagation/survival assay and counted survival cells every day. The results revealed that *INTS3*-LOF significantly reduced the numbers of survival CRC cells (Figures 3A and S3B). *INTS3*-LOF CRC cells also showed dramatically impaired colony formation capacity (Figure 3B). We also detect the function of *INTS3* in CRC self-renewal through sphere formation assay, a standard model for cancer stem cells,²⁰ and found that *INTS3* depleted CRC cells harbored an impaired sphere-forming ability (Figure 3C). These results demonstrated that *INTS3* was required for CRC survival.

We further examined the proliferation and apoptosis of *INTS3* depleted cells. Cell proliferation was detected using EdU staining assays. Unexpectedly, there was no significant difference in proliferation between *INTS3*-LOF cells and control cells (Figure 3D). Then cell apoptosis was detected with annexin V/7AAD staining, and *INTS3*-LOF resulted in a significantly increased apoptosis rate compared to control cells (Figure 3E). Moreover, the overexpression of *INTS3* increased colony formation and sphere-forming abilities of SW620 (Figures S3D and S3E) and significantly inhibited cell apoptosis (Figure S3F). Therefore, these data indicated that *INTS3* was involved in the survival regulation of CRC cells via apoptosis regulation.

INTS3 inhibits CRC apoptosis by driving the decay of pro-apoptotic transcripts

In order to investigate the molecular mechanism of *INTS3* in apoptosis regulation, RNA sequencing (RNA-seq) was performed with *INTS3* knockout and control cells, and different expressed genes (DEGs) were screened out from the transcriptomic data (Figures 4A and S4A). RNA-seq data showed that 207 genes were upregulated (Figure 4B) and 162 genes were downregulated (Figure S4B) in both sg*INTS3* #3 and sg*INTS3* #4 cells compared to control cells. The shared DEGs were then subjected to biological process analysis. Consistent with *in vitro* findings as described in Figure 3, upregulated genes in *INTS3*-LOF cells were enriched for ontologies associated with apoptotic process and positive regulation of apoptotic process (Figure 4B). Furthermore, genes associated with apoptotic process were generally upregulated in *INTS3*-LOF cells (Figure 4C) and this result was further confirmed by Gene Set Enrichment Analysis (GSEA) (Figures 4D and S4C). These RNA-seq data confirmed the requirement of *INTS3* in CRC survival and apoptosis blockade.

We further investigated the molecular mechanism of *INTS3* in apoptosis regulation. Given the obvious increase of apoptosis transcripts in *INTS3*-LOF cells, it can be predictable that *INTS3* might regulate the generation or turnover of apoptosis-associated genes. Recently, transcription-involved RBPs have been identified and these RBPs exerted their roles in nucleus via chromatin-associated RNAs. However, *INTS3* was mainly located in cytoplasm according to our immunohistochemistry data as shown in Figure 2H, diminishing the possibility of *INTS3* in transcription control. Indeed, *INTS3*-LOF cells showed comparable transcription activity to control cells, further excluding the possible

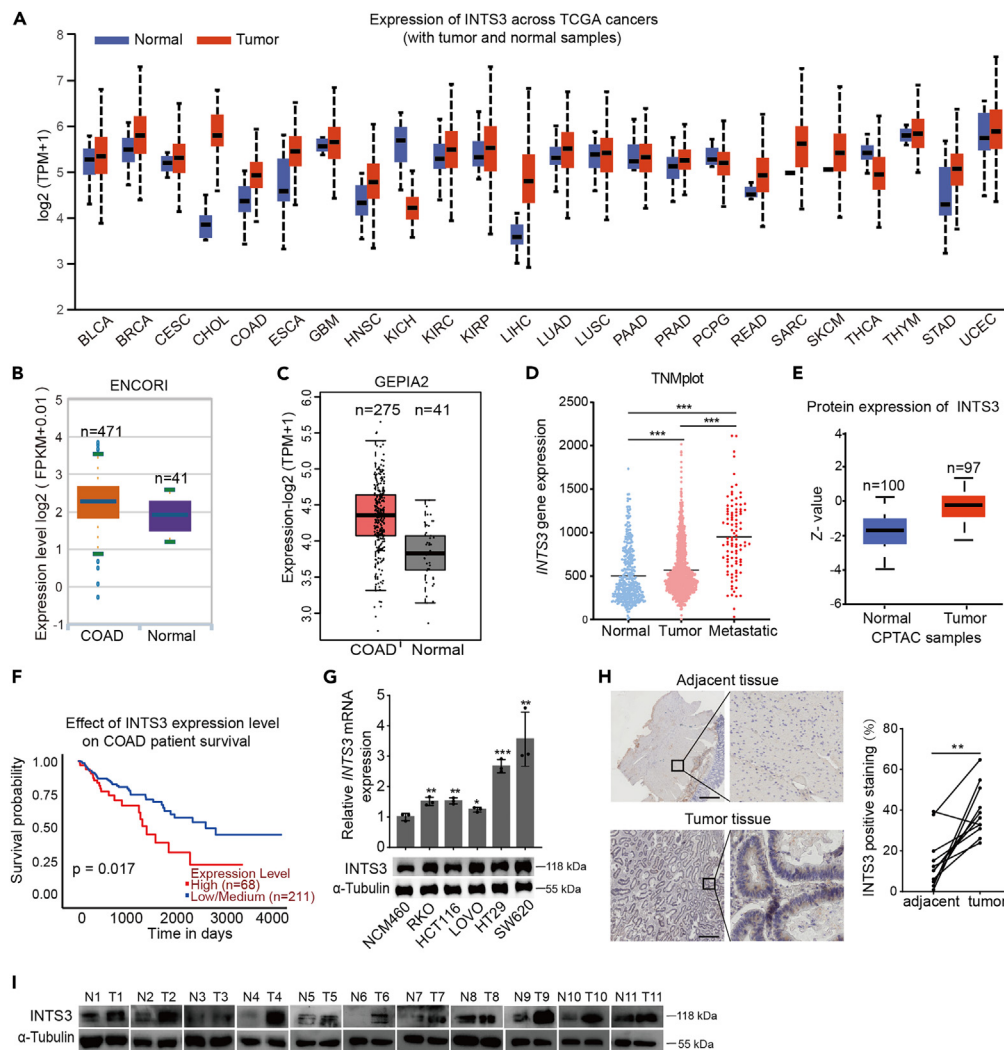


Figure 2. INTS3 is overexpressed in CRC and correlated with clinical severity

- (A) INTS3 expression in various cancer types from TCGA were validated by UALCAN.
 (B–D) ENCORI, GEPiA2, and TNMplot were analyzed for INTS3 expression levels in CRC tumor tissues and normal tissues.
 (E) Comparison of INTS3 protein expression in tumor and normal tissues of CRC in Clinical Proteomic Tumor Analysis Consortium (CPTAC) database.
 (F) Effect of INTS3 expression level on CRC patient survival. The cut-off value is the median expression of INTS3.
 (G) RT-qPCR (top) and western blot (bottom) analysis of INTS3 expression in CRC cell lines and the human normal colonic epithelial cell NCM460.
 (H) IHC analysis of INTS3 expression in 11 paired CRC patient samples. Representative images (left) and associated statistics (right).
 (I) Western blot analysis of INTS3 expression in 11 paired CRC patient samples. Scale bars: 500 μ m. * $p < 0.05$, ** $p < 0.01$, *** $p < 0.001$.

involvement of INTS3 in transcription (Figure 4E). Thus, we then detected RNA decay using RNA-seq. INTS3-LOF and the control cells were treated with actinomycin D for differential times, followed by RNA-seq (Figure 4F). Among the ten genes which were upregulated upon INTS3-LOF and enriched in “positive regulation of apoptotic process” in gene ontology (GO) analysis, five pro-apoptotic transcripts showed prolonged lifetime in INTS3-LOF samples, including NR4A1, CLU, BCL6, TXNIP, and OLFM1 (Figure 4G). Interestingly, all these five pro-apoptotic genes were down-regulated in CRC, indicating their inhibitory role in tumor propagation and survival (Figures 4H and S4D). We also confirmed the involvement of INTS3 in the stability of pro-apoptotic transcripts with RT-qPCR assay, including TXNIP, CLU, and NR4A1 mRNAs (Figure 4I). As a result, pro-apoptotic protein expression levels were upregulated in the INTS3-LOF cells (Figure 4J). These data demonstrated that INTS3 prevented CRC apoptosis through the stability of pro-apoptotic transcripts.

INTS3 depletion inhibits CRC propagation *in vivo*

To further verify the importance of INTS3 in tumor growth *in vivo*, we established a bilateral SW620 tumor model with INTS3-LOF and control tumors. Bilateral tumor-bearing mice were treated with doxycycline (DOX) for INTS3-LOF and tumors were monitored every other day.

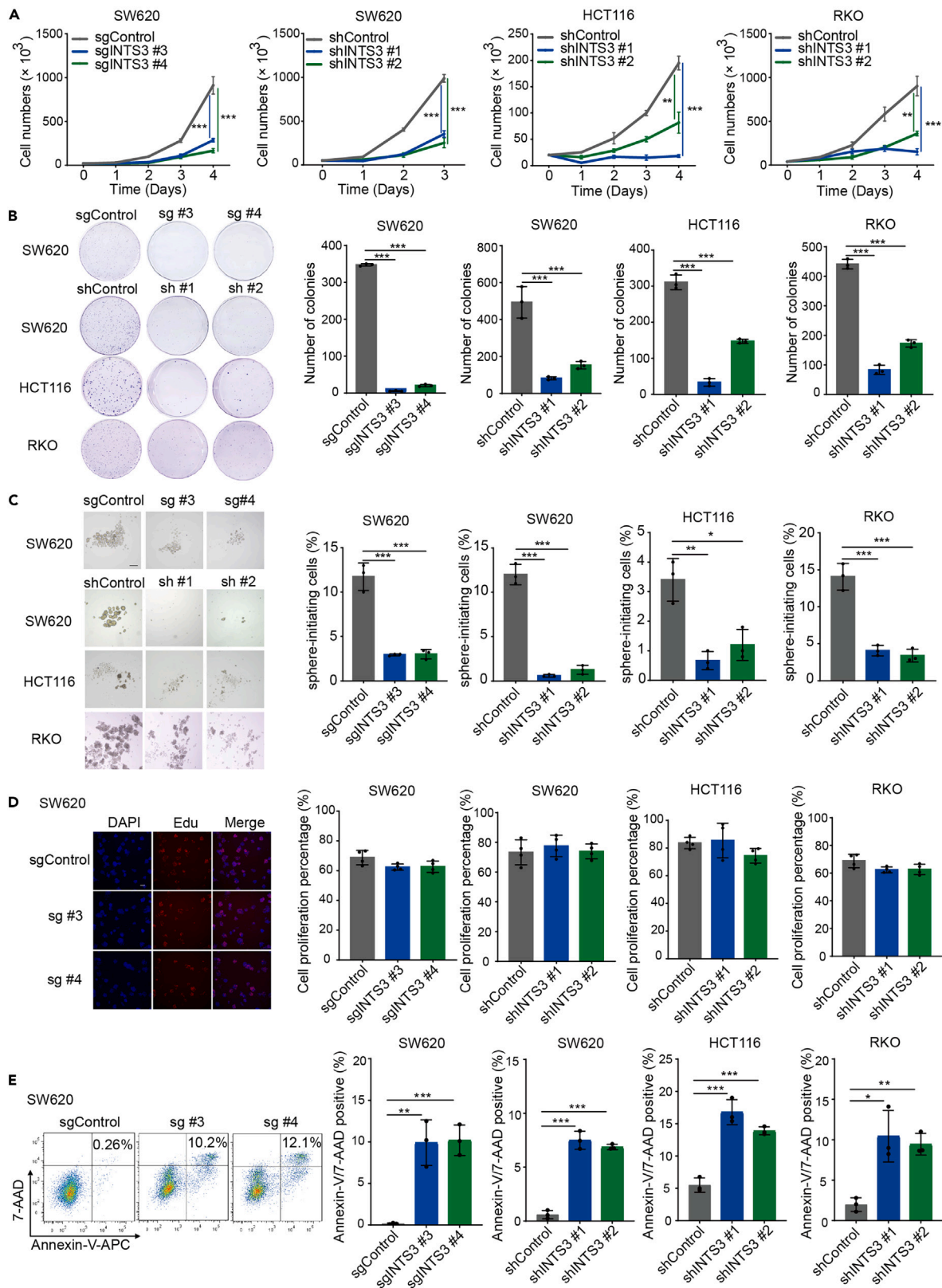


Figure 3. INTS3-LOF significantly reduces CRC cell survival

- (A) Propagation/survival assay in INTS3-LOF CRC cell lines ($n = 3$).
 (B) Colony formation assays showed the INTS3-LOF effect on clone forming ability ($n = 3$). Representative images (left) and associated statistics (right).
 (C) Sphere formation assays of INTS3-LOF and control cells ($n = 3$, scale bars: 400 μm). Representative images (left) and associated statistics (right).
 (D) EdU staining assays of INTS3-LOF and control cells ($n = 4$). Representative images (left, scale bars: 50 μm) and associated statistics (right).
 (E) Flow cytometry analysis of Annexin V/7-AAD staining of INTS3-LOF and control cells ($n = 3$). Representative images (left) and associated statistics (right).
 $*p < 0.05$, $**p < 0.01$, $***p < 0.001$.

DOX-induced INTS3 knockout significantly inhibited tumor growth compared with control tumors (Figures 5A–5D and S5A–S5D). Then bilateral HCT116 and RKO tumor models with shINTS3 and control cells were performed, and INTS3-LOF in HCT116 led to significantly decelerated tumor formation (Figures 5E, 5F, S5E, and S5F). After 20 days, tumor weights of shINTS3 group were lower than that of control group (Figures 5G and S5G), and depletion of INTS3 resulted in a satisfactory tumor regression (Figures 5H and S5H). Similarly, the bilateral RKO tumor model also showed significant tumor growth inhibition due to INTS3-LOF (Figures 5I–5L). We further confirmed that INTS3-LOF significantly induced apoptosis in CRC tumor cells with higher levels of pro-apoptotic mRNA and protein levels (Figures 5M–5P). Taken together, INTS3-LOF inhibited CRC propagation *in vivo*.

DOTAP/chol-mshINTS3 nanoparticles inhibit CT26 tumor growth *in vivo*

The tumor suppressive effects of INTS3-LOF in CRC tumor bearing mouse models demonstrated that INTS3 served as a promising target of CRC cells, and thus we sought to deliver shRNA-expressing plasmids to inhibit tumor growth *in vivo*. DOTAP/chol liposome is a promising nucleic acid delivery vehicle with satisfactory transfection efficiency.^{21,22} DOTAP/chol-based delivery vehicles have been widely used for nucleic acid delivery both preclinically and in clinical trials, with a well-established safety profile.²³ We first formulated DOTAP/chol liposome with size of 160.4 ± 0.64 nm and zeta potential of 47.6 ± 1.02 mV (Figures 6A–6C). Then, DOTAP/chol liposome was mixed with mshINTS3 plasmids at different $\mu\text{g}:\mu\text{g}$ ratios (0:1, 1:1, 2:1, 3:1, 4:1, 5:1, 6:1, 10:1) to detect suitable package rate. Agarose gel electrophoresis retardation assay showed that no free plasmid DNA was observed at a ratio of 4:1, (Figure 6D). We further detected the characterization of DOTAP/chol-mshINTS3 nanoparticles at 4:1 mixing ratio. The diameters of DOTAP/chol-mshINTS3 nanoparticle was 184.2 ± 1.5 nm, and the zeta potential of DOTAP/chol liposome switched to -12.5 ± 0.49 mV after loading mshINTS3 plasmid (Figures 6B and 6C). Based on these characterization analyses, we selected the 4:1 mixing ratio of DOTAP/chol-mshINTS3 nanoparticles in the following antitumor assays.

We established a CT26 tumor-bearing mouse model to evaluate the antitumor activity of DOTAP/chol-mshINTS3 nanoparticles *in vivo*. In this experiment, CT26 tumor cells were inoculated on the right flank of mouse (Figure 6E). One week later, the mice were randomly divided in three groups and treated with 5% glucose water, mshINTS3 plasmid or DOTAP/chol-mshINTS3 nanoparticles. No significant change in body weight was detected (Figure 6F), and hematoxylin and eosin (H&E) staining of heart, liver, spleen, lung, and kidney showed no significant damage during treatment (Figure S6A). These results demonstrated the safety of DOTAP/chol-mshINTS3 nanoparticle *in vivo*. The treatment of DOTAP/chol-mshINTS3 nanoparticle significantly reduced the INTS3 expression and had the strong effects in terms of promoting apoptotic activity (Figures S6B and S6C). Of note, DOTAP/chol-mshINTS3 nanoparticle-treated group showed a significant suppression in tumor growth, with an inhibitory rate of 86%, while mshINTS3 plasmid alone showed no obvious effect (Figures 6G–6J). These results demonstrate the effectiveness of DOTAP/chol-mshINTS3.

Generally, an attenuate tumor cell survival may be associated with the activation of anti-tumoral immunity, and here we also detected the immune cells in tumor microenvironment. Among various immune cells, CD8⁺ T cells play a central role in tumor control. Therefore, we examined the percentage and the IFN- γ -producing of intra-tumoral CD8⁺ T cells. There was no significant difference in percentage of CD8⁺ T cells among the three groups (Figure S6D). Surprisingly, we detected significantly enhanced secretion of IFN- γ in DOTAP/chol-mshINTS3 nanoparticle group, indicating the activation of anti-tumoral immune response (Figure S6E). Altogether, DOTAP/chol-mshINTS3 nanoparticles showed excellent efficiency for CRC targeting *in vivo*.

DISCUSSION

CRC remains the third most common cancer, accounting for 10% of cancer-related deaths.²⁴ The genetic and epigenetic mechanisms underlying the development and maintenance of CRC are complex.²⁵ Developing molecular targeted drugs, based on detailed mechanism exploration of key targets, are recognized as the breakthrough point in the treatment of CRC. RBPs combines with its target RNA, plays an important role in gene regulation processes such as RNA maturation, splicing, localization, and translation. Tumor cells usually have a high dependence on the RBPs due to active RNA synthesis, indicating that RBPs are excellent target for the treatment of CRC.^{26,27} Our RBPs CRISPR-Cas9 screening enabled the systematic discovery of RBPs served as driver genes of CRC tumorigenesis and survival. A total of 27 critical RBPs which closely related to the survival of CRC were screened out, involved in tRNA aminoacylation for protein translation, mitochondrial translation, ncRNA processing, mRNA splicing and translation. Among the screened RBPs, INTS3 ranked first, and was less studied on CRC.

INTS3 is one of the subunits of integrator complex, and has been reported to regulate the mRNA transcription and processing.²⁸ Many researches have demonstrated that abnormal integrator subsets contribute to tumorigenesis in multiple tumor types.²⁹ For example, INTS6 is found to inhibit hepatocellular carcinoma growth by increasing WIF-1 mRNA levels.³⁰ We found that INTS3 was overexpressed in CRC patients and tumor cell lines, and inhibited CRC apoptosis by driving the decay of pro-apoptotic gene transcripts. According to the experiment

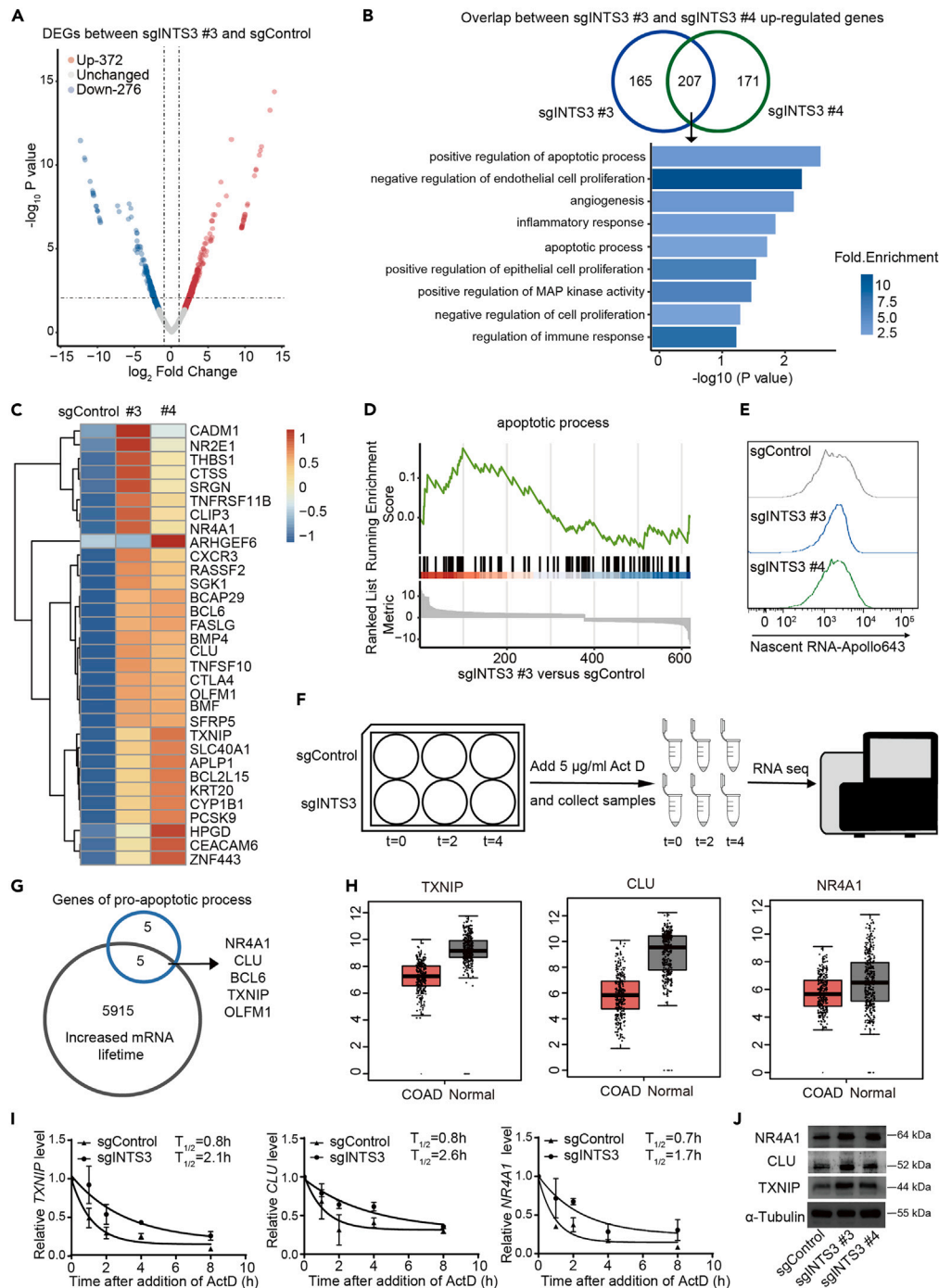


Figure 4. INTS3 reduces the expression of pro-apoptotic genes by regulating mRNA stability

(A) Volcano plot of RNA-seq data showing the distribution of mapped different expressed genes (DEGs) between sgINTS3 #3 and sgControl.

(B) Overlap between sgINTS3 #3 and sgINTS3 #4 upregulated genes (top). Biological process analysis of overlap genes (bottom).

(C) Heatmap of upregulated genes in apoptotic process from the RNA-seq experiment.

(D) Gene Set Enrichment Analysis (GSEA) was used to analyze the distribution of differentially expressed genes between sgINTS3 #3 and sgControl in apoptotic process.

(E) Nascent RNA labeling assay.

(F) Schematic of RNA stability assay.

Figure 4. Continued

- (G) Overlap between ten pro-apoptotic genes and genes with extended mRNA half-life (lifetime_{sgINTS3 #4}/lifetime_{control} > 1.5).
 (H) TXNIP, CLU, and NR4A1 expression levels in CRC tumor tissues and normal tissues.
 (I) After treatment of SW620 cells with 5 μg/mL ActD for 0, 1, 2, 4, and 8 h, the effects of INTS3 knockout on TXNIP, CLU, and NR4A1 mRNA stability (n = 3).
 (J) Western blot analysis of TXNIP, CLU, and NR4A1 expression.

results *in vitro* and *in vivo*, the loss of INTS3 significantly increased the CRC cells apoptosis rate by regulating mRNA stability of pro-apoptotic genes TXNIP, NR4A1, and CLU. TXNIP has been identified as a tumor suppressor gene and the low level of TXNIP expression is correlated with poor prognosis.^{31,32} Pro-survival BCL-2 proteins restrain the effectors of apoptosis in tumors.³³ Accumulating evidence suggests that NR4A1, the target gene of INTS3 in our results, can convert Bcl-2 from protector to a killer, thereby promoting tumor cells apoptosis.^{34,35} Another target gene CLU has been proved to promotes apoptosis in CRC and prostate cancer by the nuclear form.^{36,37}

INTS3-LOF inhibits CRC growth propagation *in vivo*, indicating INTS3 is an excellent intervention target for the treatment of CRC. Nucleic acid delivery systems are mainly divided into viral vectors or non-viral vectors. Cationic liposomes are the most used non-viral gene transfer systems.³⁸ DOTAP/chol lipid nanoparticles have the advantages of low toxicity, biodegradability, easy synthesis, and low immunoreactivity, and have been studied for the delivery of plasmid DNA, mRNA, small interfering RNA, microRNA, or antisense oligonucleotides.³⁹ More importantly, DOTAP-based lipid nanoparticles have been intensively investigated in clinical trials.^{40–43} After clarifying the role mechanism of INTS3 in CRC survival support, our research focused on the delivery of RNA-interference drugs in CRC cells. The results showed that DOTAP/cholesterol-mshINTS3 nanoparticles can significantly inhibit CT26 tumor growth but have no security risks *in vivo*, indicating that DOTAP/chol-mshINTS3 nanoparticles have enormous potential application value in the treatment of CRC.

Limitations of the study

We performed a CRISPR-Cas9 screening using an RBP-pooled CRISPR knockout library and identified 27 potential RBPs for supporting CRC survival, including a function-undefined INTS3. We found that INTS3 prevented CRC apoptosis through the stability of pro-apoptotic transcripts, but we did not study the mechanisms of the regulation of pro-apoptotic transcripts stability by INTS3. Our study also showed that CRC tumor growth was inhibited by the intratumoral injection delivery of DOTAP/chol-mshINTS3 nanoparticle, but there are some challenges for clinical implementation of intratumoral injections, such as the injectability. Further research is needed to increase the tumor targeting capability of DOTAP/chol-mshINTS3 nanoparticle.

STAR★METHODS

Detailed methods are provided in the online version of this paper and include the following:

- **KEY RESOURCES TABLE**
- **RESOURCE AVAILABILITY**
 - Lead contact
 - Materials availability
 - Data and code availability
- **EXPERIMENTAL MODEL AND STUDY PARTICIPANT DETAILS**
 - Cell culture
 - Mice
 - Clinical samples
- **METHOD DETAILS**
 - RBP pooled CRISPR knockout library amplification and lentivirus package
 - RBP CRISPR-cas9 screening
 - Immunohistochemistry (IHC) staining assay
 - sgRNA, shRNA and overexpression cell lines
 - Propagation/survival assay of human CRC cells
 - Annexin V-APC/7-AAD apoptosis assay
 - Cell proliferation assay
 - *In vivo* transplantation of human CRC cell lines
 - mRNA sequencing
 - Nascent RNA labeling
 - RNA stability assay
 - RNA isolation, reverse transcription and RT-qPCR
 - DOTAP/cholesterol liposome preparation and characterization
 - DOTAP/chol-mshINTS3 nanoparticle antitumor assay *in vivo*
- **QUANTIFICATION AND STATISTICAL ANALYSIS**

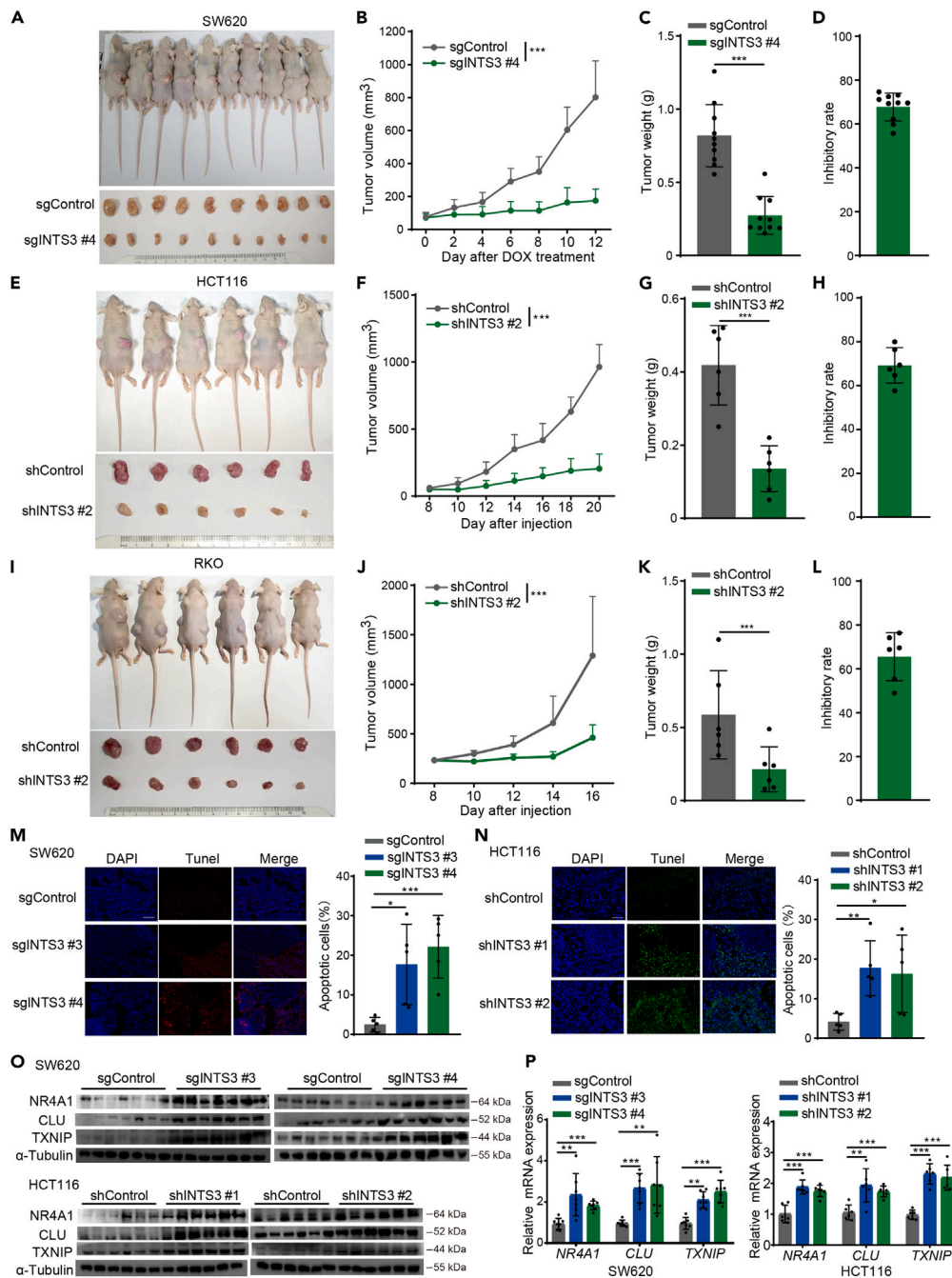


Figure 5. INTS3 depletion inhibits CRC propagation in vivo

(A) Images of SW620-transduced cell tumor-bearing mice treated with DOX drinking water for 12 days (top). sgINTS3 #4 and control tumor tissues (bottom). (B–D) The growth curves (B), tumor weight (C), and tumor inhibition rate (D) of sgINTS3 #4 and control SW620 cell tumors ($n = 10$). (E) Images of HCT116-transduced cell tumor-bearing mice (top). shINTS3 #2 and control tumor tissues (bottom). (F–H) The growth curves (F), tumor weight (G), and tumor inhibition rate (H) of shINTS3 #2 and control HCT116 cell tumors ($n = 6$). (I) Images of RKO-transduced cell tumor-bearing mice (top). INTS3-LOF and control tumor tissues (bottom). (J–L) The growth curves (J), tumor weight (K), and tumor inhibition rate (L) of shINTS3 #2 and control RKO cell tumors ($n = 6$). (M and N) TUNEL staining showed the SW620 (M) and HCT116 (N) tumor cell apoptosis in each group ($n = 5$, scale bars: 50 μm). (O) Western blot analysis of TXNIP, CLU, and NR4A1 protein expression. SW620 tumor tissues (top, $n = 7$) and HCT116 tumor tissues (bottom, $n = 6$). (P) RT-qPCR analysis of TXNIP, CLU, and NR4A1 mRNA expression. SW620 tumor tissues (left, $n = 7$) and HCT116 tumor tissues (right, $n = 6$). * $p < 0.05$, ** $p < 0.01$, *** $p < 0.001$.

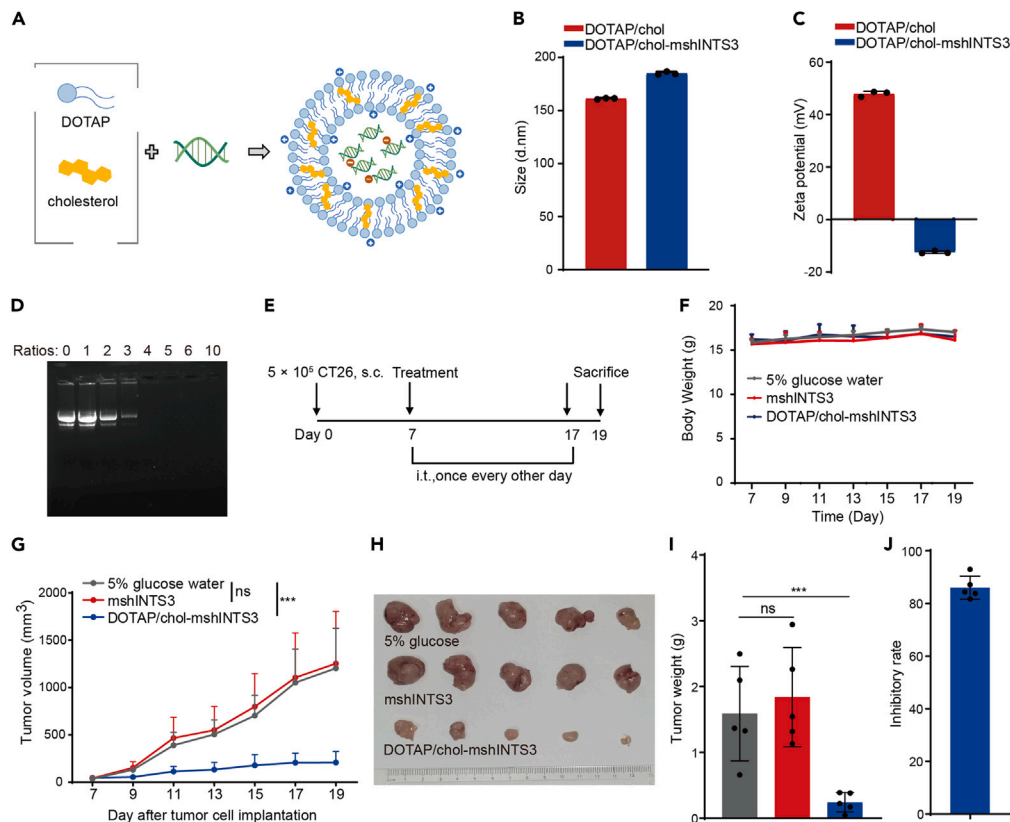


Figure 6. DOTAP/chol-mshINTS3 nanoparticle therapy inhibit CT26 tumor growth *in vivo*

(A) Schematic of shRNA-expression plasmid delivery system based on DOTAP/chol liposomes.
 (B) The hydrodynamic size of DOTAP/chol and DOTAP/chol-mshINTS3 ($\mu\text{g}:\mu\text{g} = 4:1$) nanoparticles ($n = 3$).
 (C) The zeta-potential of DOTAP/chol and DOTAP/chol-mshINTS3 ($\mu\text{g}:\mu\text{g} = 4:1$) nanoparticles ($n = 3$).
 (D) Agarose gel electrophoresis retardation assay of DOTAP/Chol-mshINTS3 nanoparticles at different $\mu\text{g}:\mu\text{g}$ ratios (DOTAP/Chol: mshINTS3 = 0:1, 1:1, 2:1, 3:1, 4:1, 5:1, 6:1, 10:1).
 (E) Schematic of DOTAP/Chol-mshINTS3 nanoparticle therapy in the CT26 tumor model.
 (F) Body weight curves of mice during treatment ($n = 5$).
 (G) The growth curves of tumors treated with different treatments (5% glucose water, plasmid of shINTS3 and DOTAP/chol-mshINTS3 nanoparticles, $n = 5$).
 (H) Images of the tumor tissues of different groups at day 19 ($n = 5$).
 (I) Tumor weight of different groups ($n = 5$).
 (J) Tumor inhibition rate of CT26-bearing mice after treatment with DOTAP/chol-mshINTS3 nanoparticle ($n = 5$). $***p < 0.001$.

SUPPLEMENTAL INFORMATION

Supplemental information can be found online at <https://doi.org/10.1016/j.isci.2024.109676>.

ACKNOWLEDGMENTS

This work was supported by the Ministry of Science and Technology of the People's Republic of China (grant number 2020YFA0803500 to P.Z.) and National Natural Science Foundation of China (grant numbers 82173176 to P.Z. and 32200652 to Q.H.).

AUTHOR CONTRIBUTIONS

P.Z., Q.H., and Z.C. designed the study and reviewed the manuscript; P.Z. and Q.H. provided funding support; Zhiwei Wang, C.Z., J.G., P.L., S.L., L.Z., X.Z., and X.W. carried out the experiments; Y.Y., Ziyang Wang, and J.Z. performed the statistical analysis; Q.Z. participated in the clinical sample detection; Zhiwei Wang and C.Z. wrote and revised the manuscript. All authors read and approved the final manuscript.

DECLARATION OF INTERESTS

The authors declare no competing interests.

Received: December 3, 2023

Revised: February 17, 2024

Accepted: April 3, 2024

Published: April 6, 2024

REFERENCES

1. Siegel, R.L., Miller, K.D., Wagle, N.S., and Jemal, A. (2023). Cancer statistics, 2023. *CA A Cancer J. Clin.* 73, 17–48. <https://doi.org/10.3322/caac.21763>.
2. Siegel, R.L., Wagle, N.S., Cercek, A., Smith, R.A., and Jemal, A. (2023). Colorectal cancer statistics, 2023. *CA A Cancer J. Clin.* 73, 233–254. <https://doi.org/10.3322/caac.21772>.
3. Zhou, H., Liu, Z., Wang, Y., Wen, X., Amador, E.H., Yuan, L., Ran, X., Xiong, L., Ran, Y., Chen, W., and Wen, Y. (2022). Colorectal liver metastasis: molecular mechanism and interventional therapy. *Signal Transduct. Targeted Ther.* 7, 70. <https://doi.org/10.1038/s41392-022-00922-2>.
4. Du, L., Cheng, Q., Zheng, H., Liu, J., Liu, L., and Chen, Q. (2022). Targeting stemness of cancer stem cells to fight colorectal cancers. *Semin. Cancer Biol.* 82, 150–161. <https://doi.org/10.1016/j.semcancer.2021.02.012>.
5. Xie, Y.H., Chen, Y.X., and Fang, J.Y. (2020). Comprehensive review of targeted therapy for colorectal cancer. *Signal Transduct. Targeted Ther.* 5, 22. <https://doi.org/10.1038/s41392-020-0116-z>.
6. Lambert, S.A., Jolma, A., Campitelli, L.F., Das, P.K., Yin, Y., Albu, M., Chen, X., Taipale, J., Hughes, T.R., and Weirauch, M.T. (2018). The Human Transcription Factors. *Cell* 172, 650–665. <https://doi.org/10.1016/j.cell.2018.01.029>.
7. Xiao, R., Chen, J.Y., Liang, Z., Luo, D., Chen, G., Lu, Z.J., Chen, Y., Zhou, B., Li, H., Du, X., et al. (2019). Pervasive Chromatin-RNA Binding Protein Interactions Enable RNA-Based Regulation of Transcription. *Cell* 178, 107–121.e18. <https://doi.org/10.1016/j.cell.2019.06.001>.
8. Liu, J., Dou, X., Chen, C., Chen, C., Liu, C., Xu, M.M., Zhao, S., Shen, B., Gao, Y., Han, D., and He, C. (2020). N(6)-methyladenosine of chromosome-associated regulatory RNA regulates chromatin state and transcription. *Science* 367, 580–586. <https://doi.org/10.1126/science.aay6018>.
9. Hong, S. (2017). RNA Binding Protein as an Emerging Therapeutic Target for Cancer Prevention and Treatment. *J. Cancer Prev.* 22, 203–210. <https://doi.org/10.15430/JCP.2017.22.4.203>.
10. Pereira, B., Billaud, M., and Almeida, R. (2017). RNA-Binding Proteins in Cancer: Old Players and New Actors. *Trends Cancer* 3, 506–528. <https://doi.org/10.1016/j.trecan.2017.05.003>.
11. Chen, Z., Huang, L., Wang, K., Zhang, L., Zhong, X., Yan, Z., Liu, B., and Zhu, P. (2022). rtcisE2F promotes the self-renewal and metastasis of liver tumor-initiating cells via N(6)-methyladenosine-dependent E2F3/E2F6 mRNA stability. *Sci. China Life Sci.* 65, 1840–1854. <https://doi.org/10.1007/s11427-021-2038-5>.
12. Chen, Z., Wu, J., Liu, B., Zhang, G., Wang, Z., Zhang, L., Wang, K., Fan, Z., and Zhu, P. (2021). Identification of cis-HOX-HOX10 axis as a therapeutic target for colorectal tumor-initiating cells without APC mutations. *Cell Rep.* 36, 109431. <https://doi.org/10.1016/j.celrep.2021.109431>.
13. Haley, B., and Roudnicki, F. (2020). Functional Genomics for Cancer Drug Target Discovery. *Cancer Cell* 38, 31–43. <https://doi.org/10.1016/j.ccell.2020.04.006>.
14. Katti, A., Diaz, B.J., Caragine, C.M., Sanjana, N.E., and Dow, L.E. (2022). CRISPR in cancer biology and therapy. *Nat. Rev. Cancer* 22, 259–279. <https://doi.org/10.1038/s41568-022-00441-w>.
15. Wheeler, E.C., Vu, A.Q., Einstein, J.M., DiSalvo, M., Ahmed, N., Van Nostrand, E.L., Shishkin, A.A., Jin, W., Allbritton, N.L., and Yeo, G.W. (2020). Pooled CRISPR screens with imaging on microarray reveals stress granule-regulatory factors. *Nat. Methods* 17, 636–642. <https://doi.org/10.1038/s41592-020-0826-8>.
16. Lin, J., Yu, X., Xie, L., Wang, P., Li, T., Xiao, Y., Zhou, J., Peng, S., Huang, J., Luo, Y., et al. (2019). eIF6 Promotes Colorectal Cancer Proliferation and Invasion by Regulating AKT-Related Signaling Pathways. *J. Biomed. Nanotechnol.* 15, 1556–1567. <https://doi.org/10.1166/jbnn.2019.2792>.
17. Zhou, T., Wu, L., Ma, N., Tang, F., Yu, Z., Jiang, Z., Li, Y., Zong, Z., and Hu, K. (2020). SOX9-activated FARS1-AS1 predetermines cell growth, stemness, and metastasis in colorectal cancer through upregulating FARS1 and SOX9. *Cell Death Dis.* 11, 1071. <https://doi.org/10.1038/s41419-020-03273-4>.
18. Chen, Y., Hou, W., Zhong, M., and Wu, B. (2021). Comprehensive Proteomic Analysis of Colon Cancer Tissue Revealed the Reason for the Worse Prognosis of Right-Sided Colon Cancer and Mucinous Colon Cancer at the Protein Level. *Curr. Oncol.* 28, 3554–3572. <https://doi.org/10.3390/curroncol28050305>.
19. Vaughan-Shaw, P.G., Blackmur, J.P., Grimes, G., Ooi, L.Y., Ochocka-Fox, A.M., Dunbar, K., von Kriegsheim, A., Rajasekaran, V., Timofeeva, M., Walker, M., et al. (2022). Vitamin D treatment induces *in vitro* and *ex vivo* transcriptomic changes indicating anti-tumor effects. *Faseb. J.* 36, e22082. <https://doi.org/10.1096/fj.202101430RR>.
20. Zhu, P., Lu, T., Chen, Z., Liu, B., Fan, D., Li, C., Wu, J., He, L., Zhu, X., Du, Y., et al. (2022). 5-hydroxytryptamine produced by enteric serotonergic neurons initiates colorectal cancer stem cell self-renewal and tumorigenesis. *Neuron* 110, 2268–2282.e4. <https://doi.org/10.1016/j.neuron.2022.04.024>.
21. Kim, S.Y., Lee, S.J., and Lim, S.J. (2014). Formulation and *in vitro* and *in vivo* evaluation of a cationic emulsion as a vehicle for improving adenoviral gene transfer. *Int. J. Pharm.* 475, 49–59. <https://doi.org/10.1016/j.ijpharm.2014.08.024>.
22. Shen, L., Li, J., Liu, Q., Song, W., Zhang, X., Tiruthani, K., Hu, H., Das, M., Goodwin, T.J., Liu, R., and Huang, L. (2018). Local Blockade of Interleukin 10 and C-X-C Motif Chemokine Ligand 12 with Nano-Delivery Promotes Antitumor Response in Murine Cancers. *ACS Nano* 12, 9830–9841. <https://doi.org/10.1021/acsnano.8b00967>.
23. Miao, L., Zhang, Y., and Huang, L. (2021). mRNA vaccine for cancer immunotherapy. *Mol. Cancer* 20, 41. <https://doi.org/10.1186/s12943-021-01335-5>.
24. Dekker, E., Tanis, P.J., Vleugels, J.L.A., Kasi, P.M., and Wallace, M.B. (2019). Colorectal cancer. *Lancet* 394, 1467–1480. [https://doi.org/10.1016/S0140-6736\(19\)32319-0](https://doi.org/10.1016/S0140-6736(19)32319-0).
25. Grazioso, T.P., Brandt, M., and Djouder, N. (2019). Diet, Microbiota, and Colorectal Cancer. *iScience* 21, 168–187. <https://doi.org/10.1016/j.isci.2019.10.011>.
26. Qin, H., Ni, H., Liu, Y., Yuan, Y., Xi, T., Li, X., and Zheng, L. (2020). RNA-binding proteins in tumor progression. *J. Hematol. Oncol.* 13, 90. <https://doi.org/10.1186/s13045-020-00927-w>.
27. Wang, S., Sun, Z., Lei, Z., and Zhang, H.T. (2022). RNA-binding proteins and cancer metastasis. *Semin. Cancer Biol.* 86, 748–768. <https://doi.org/10.1016/j.semcancer.2022.03.018>.
28. Skaar, J.R., Ferris, A.L., Wu, X., Saraf, A., Khanna, K.K., Florens, L., Washburn, M.P., Hughes, S.H., and Pagano, M. (2015). The Integrator complex controls the termination of transcription at diverse classes of gene targets. *Cell Res.* 25, 288–305. <https://doi.org/10.1038/cr.2015.19>.
29. Welsh, S.A., and Gardini, A. (2023). Genomic regulation of transcription and RNA processing by the multitasking Integrator complex. *Nat. Rev. Mol. Cell Biol.* 24, 204–220. <https://doi.org/10.1038/s41580-022-00534-2>.
30. Lui, K.Y., Zhao, H., Qiu, C., Li, C., Zhang, Z., Peng, H., Fu, R., Chen, H.A., and Lu, M.Q. (2017). Integrator complex subunit 6 (INTS6) inhibits hepatocellular carcinoma growth by Wnt pathway and serve as a prognostic marker. *BMC Cancer* 17, 644. <https://doi.org/10.1186/s12885-017-3628-3>.
31. Chen, Y., Ning, J., Cao, W., Wang, S., Du, T., Jiang, J., Feng, X., and Zhang, B. (2020). Research Progress of TXNIP as a Tumor Suppressor Gene Participating in the Metabolic Reprogramming and Oxidative Stress of Cancer Cells in Various Cancers. *Front. Oncol.* 10, 568574. <https://doi.org/10.3389/fonc.2020.568574>.
32. Deng, J., Pan, T., Liu, Z., McCarthy, C., Vicencio, J.M., Cao, L., Alfano, G., Suwaidan, A.A., Yin, M., Beatson, R., and Ng, T. (2023). The role of TXNIP in cancer: a fine balance between redox, metabolic, and immunological tumor control. *Br. J. Cancer* 129, 1877–1892. <https://doi.org/10.1038/s41416-023-02442-4>.
33. Kaloni, D., Diepstraten, S.T., Strasser, A., and Kelly, G.L. (2023). BCL-2 protein family: attractive targets for cancer therapy. *Apoptosis* 28, 20–38. <https://doi.org/10.1007/s10495-022-01780-7>.
34. Lin, B., Kolluri, S.K., Lin, F., Liu, W., Han, Y.H., Cao, X., Dawson, M.I., Reed, J.C., and Zhang, X.K. (2004). Conversion of Bcl-2 from protector to killer by interaction with nuclear

- orphan receptor Nur77/TR3. *Cell* 116, 527–540. [https://doi.org/10.1016/s0092-8674\(04\)00162-x](https://doi.org/10.1016/s0092-8674(04)00162-x).
35. Deutsch, A.J.A., Rinner, B., Wenzl, K., Pichler, M., Troppan, K., Steinbauer, E., Schwarzenbacher, D., Reitter, S., Feichtinger, J., Tierling, S., et al. (2014). NR4A1-mediated apoptosis suppresses lymphomagenesis and is associated with a favorable cancer-specific survival in patients with aggressive B-cell lymphomas. *Blood* 123, 2367–2377. <https://doi.org/10.1182/blood-2013-08-518878>.
 36. Dia, V.P., and Mejia, E.G.d. (2010). Lunasin promotes apoptosis in human colon cancer cells by mitochondrial pathway activation and induction of nuclear clusterin expression. *Cancer Lett.* 295, 44–53. <https://doi.org/10.1016/j.canlet.2010.02.010>.
 37. Shannan, B., Seifert, M., Boothman, D.A., Tilgen, W., and Reichrath, J. (2007). Clusterin over-expression modulates proapoptotic and antiproliferative effects of 1,25(OH)2D3 in prostate cancer cells *in vitro*. *J. Steroid Biochem. Mol. Biol.* 103, 721–725. <https://doi.org/10.1016/j.jsbmb.2006.12.068>.
 38. Yin, H., Kanasty, R.L., Eltoukhy, A.A., Vegas, A.J., Dorkin, J.R., and Anderson, D.G. (2014). Non-viral vectors for gene-based therapy. *Nat. Rev. Genet.* 15, 541–555. <https://doi.org/10.1038/nrg3763>.
 39. Ruponen, M., Honkakoski, P., Rönkkö, S., Pelkonen, J., Tammi, M., and Urtili, A. (2003). Extracellular and intracellular barriers in non-viral gene delivery. *J. Contr. Release* 93, 213–217. <https://doi.org/10.1016/j.jconrel.2003.08.004>.
 40. Porteous, D.J., Dorin, J.R., McLachlan, G., Davidson-Smith, H., Davidson, H., Stevenson, B.J., Carothers, A.D., Wallace, W.A., Moralee, S., Hoenes, C., et al. (1997). Evidence for safety and efficacy of DOTAP cationic liposome mediated CFTR gene transfer to the nasal epithelium of patients with cystic fibrosis. *Gene Ther.* 4, 210–218. <https://doi.org/10.1038/sj.gt.3300390>.
 41. Lu, C., Stewart, D.J., Lee, J.J., Ji, L., Ramesh, R., Jayachandran, G., Nunez, M.I., Wistuba, I.I., Erasmus, J.J., Hicks, M.E., et al. (2012). Phase I clinical trial of systemically administered TUSC2(FUS1)-nanoparticles mediating functional gene transfer in humans. *PLoS One* 7, e34833. <https://doi.org/10.1371/journal.pone.0034833>.
 42. Piowarczyk, L., Mlynarczyk, D.T., Krajka-Kuźniak, V., Majchrzak-Celińska, A., Budzianowska, A., Tomczak, S., Budzianowski, J., Woźniak-Braszak, A., Pietrzyk, R., Baranowski, M., et al. (2022). Natural Compounds in Liposomal Nanoformulations of Potential Clinical Application in Glioblastoma. *Cancers* 14, 6222. <https://doi.org/10.3390/cancers14246222>.
 43. Hadinoto, K., Sundaresan, A., and Chew, W.S. (2013). Lipid-polymer hybrid nanoparticles as a new generation therapeutic delivery platform: a review. *Eur. J. Pharm. Biopharm.* 85, 427–443. <https://doi.org/10.1016/j.ejpb.2013.07.002>.
 44. Wang, B., Wang, M., Zhang, W., Xiao, T., Chen, C.H., Wu, A., Wu, F., Traugh, N., Wang, X., Li, Z., et al. (2019). Integrative analysis of pooled CRISPR genetic screens using MAGeCKFlute. *Nat. Protoc.* 14, 756–780. <https://doi.org/10.1038/s41596-018-0113-7>.

STAR★METHODS

KEY RESOURCES TABLE

REAGENT or RESOURCE	SOURCE	IDENTIFIER
Antibodies		
INTS3 antibody	Proteintech	Cat#16620-1-AP; RRID:AB_2127274
TXNIP Antibody	MedChemExpress	Cat#HY-P80361; RRID:AB_3094610
Anti-NR4A1 rabbit polyclonal antibody	Sangon Biotech	Cat#D222799; RRID:AB_3094612
Anti-CLU rabbit polyclonal antibody	Sangon Biotech	Cat#D262659; RRID:AB_3094611
α -Tubulin Rabbit mAb	CellSignalingTechnology	Cat#2125; RRID:AB_2619646
CD45 Monoclonal Antibody (30-F11), FITC	Thermofisher Scientific	Cat#11-0451-82; RRID:AB_465050
CD3 Monoclonal Antibody (17A2), PerCP-eFluor™ 710	Thermofisher Scientific	Cat# 46-0032-82; RRID:AB_1834427
IFN gamma Monoclonal Antibody (XMG1.2), APC	Thermofisher Scientific	Cat# 17-7311-82; RRID:AB_469504
BD Horizon™ BV605 Rat Anti-Mouse CD8a	BD biosciences	Cat#563152; RRID:AB_2738030
Bacterial and virus strains		
E. cloni 10G Supreme Electrocompetent Cells	LGC, Biosearch Technologies	Cat# 60081-1
Biological samples		
Human CRC samples	The First Affiliated Hospital of Zhengzhou University	https://www.zdyfy.com/home
Chemicals, peptides, and recombinant proteins		
Puromycin	Thermofisher Scientific	Cat#A1113802
Doxycycline	Solarbio Life Sciences	Cat#D8960
TritonX-100	Solarbio Life Sciences	Cat#IT9100
ActinomycinD	MedChemExpress	HY-17559
VeZol reagent	Vazyme	Cat#R411-01
DOTAP	MACKLIN	Cat#D890287
Cholesterol	MedChemExpress	Cat#HY-N0322
Ionomycin	Sigma	Cat#407951
Protein transport inhibitor	BD biosciences	Cat#555029
PMA	Sigma	Cat#P8139
Critical commercial assays		
FastPure Gel DNA Extraction Mini Kit	Vazyme	Cat#DC301-01
FastPure EndoFree Plasmid Maxi Kit	Vazyme	Cat#DC202-01
MiniBEST Universal Genomic DNA Extraction Kit	Takara Biomedical Technology	Cat#9765
Annexin V-APC/7-AAD Apoptosis Kit	Procell	Cat#P-CA-208
EdU Cell Proliferation Kit with Alexa Fluor 647	Beyotime	Cat#C0081S
Cell-Light EU Apollo643 RNA Imaging Kit	RiboBio	Cat#C10316-2
HiScript III RT SuperMix	Vazyme	Cat#R323-01
AceQ Universal SYBR qPCR Master Mix	Vazyme	Cat#Q511-02
Phanta Super-Fidelity DNA Polymerase	Vazyme	Cat#P501-d2
HiEff Trans® Liposomal Transfection Reagent	Yeasen Biotechnology	Cat#40802ES02
Experimental models: Cell lines		
SW620	ATCC	Cat#CCL-227; RRID:CVCL_0547
RKO	ATCC	Cat#CRL-2577; RRID:CVCL_0504

(Continued on next page)

Continued		
REAGENT or RESOURCE	SOURCE	IDENTIFIER
HCT116	Pricella	Cat#CL-0096;
CT26	ATCC	Cat#CRL-2638; RRID:CVCL_7256
HEK-293T	ATCC	Cat#CRL-3216; RRID:CVCL_0063
Experimental models: Organisms/strains		
BALB/c nude mice	Beijing Sibeifu	N/A
BALB/c mice	Beijing Sibeifu	N/A
Oligonucleotides		
β-actin forward: CCTGGCACCCAGCACAAT	This paper	N/A
β-actin reverse: GGGCCGGACTCGTCATACT	This paper	N/A
INTS3 forward: AACTGGTGAAGAGTGGGGTTC	This paper	N/A
INTS3 reverse: GGAGGTACGTGTAAACAGCCAT	This paper	N/A
NR4A1 forward: GCTACGAACTTGGGGGAGT	This paper	N/A
NR4A1 reverse: GAGAATCCGGCTTCAGGCAG	This paper	N/A
BCL6 forward: TCTAGGAAAGCCGGACACC	This paper	N/A
BCL6 reverse: AAAGTCTCACGGCTCACAA	This paper	N/A
TXNIP forward: TCCAGCAATTGGGGGAAAGA	This paper	N/A
TXNIP reverse: CTCCAAATCGAGGAAACCCCT	This paper	N/A
CLU forward: CCCACACTTCTGACTCGGAC	This paper	N/A
CLU reverse: CCCGTAGGTGCAAAAGCAAC	This paper	N/A
OLFM1 forward: AACTGGATGTCCCAGACGCT	This paper	N/A
OLFM1 reverse: AGCGACCACTGTGCAGATAC	This paper	N/A
Recombinant DNA		
RNA-Binding Protein Pooled CRISPR Knockout Library	Addgene	Cat#141438
TLCV2	Addgene	Cat#87360
pSicoR-mCh-empty	Addgene	Cat#21907
pLVX-puro	HedgehogBio	Cat#HH-LV-048
pMD2.G	Addgene	Cat#12259
psPAX2	Addgene	Cat#12260
Software and algorithms		
ImageJ	NIH	https://imagej.nih.gov/ij/
MAGeCK	Li et al.	https://sourceforge.net/projects/mageck/
Other		
FACSymphony S6 system	BD Biosciences	N/A
CX7LZR high-content analysis platform	Thermo Scientific	N/A
Malvern Instrument	Malvern	N/A

RESOURCE AVAILABILITY

Lead contact

Further information and requests for resources and reagents should be directed to and will be fulfilled by the lead contact, Qiankun He (email: qiankunhe@zzu.edu.cn).

Materials availability

This study did not generate new unique reagents and all materials in this study are commercially available.

Data and code availability

- Data reported in this paper will be shared by the [lead contact](#) upon request.

- This paper does not report original code.
- Any additional information required to reanalyze the data reported in this paper is available from the [lead contact](#) upon request.

EXPERIMENTAL MODEL AND STUDY PARTICIPANT DETAILS

Cell culture

SW620, RKO, CT26 cells were cultured in RPMI1640 medium (Gibco). HEK-293T and HCT116 were cultured in Dulbecco's modified Eagle's medium (DMEM) medium (Gibco). All media were supplemented with 10% FBS (Lonsera) and 1% penicillin-streptomycin. All cells were incubated at 37°C with 5% CO₂.

Mice

5-7-week-old male BALB/c nude mice and male BALB/c mice were purchased from the Sipeifu Bioscience Co. Inc (Beijing, China). Mice were maintained in the specific pathogen-free facility at Zhengzhou University. The animal experiments were approved by Ethics Committee of Zhengzhou University (ZZUIRB2020-54).

Clinical samples

CRC tumor and paired normal adjacent samples were obtained from The First Affiliated Hospital of Zhengzhou University. All experimental procedures were approved by Ethics Committee of Zhengzhou University (ZZUIRB2020-54). Written informed consents were obtained from all patients.

METHOD DETAILS

RBP pooled CRISPR knockout library amplification and lentivirus package

RBP pooled CRISPR knockout library (Addgene, #141438) contains 10,774 individual gRNAs for RBPs, 1,058 negative control gRNAs and 628 positive gRNAs targeting essential genes. Library plasmids were extracted and removed endotoxin using FastPure EndoFree Plasmid Maxi Kit (Vazyme, DC202-01).

HEK293T cells were seeded on six 15 cm culture dishes at 70% confluency. The medium was replaced with serum-free DMEM before lentivirus package. Each package program was performed using 150 μL Hieff Trans® Liposomal Transfection Reagent (Yeasen Biotechnology, 40802ES02), 30 μg RBP CRISPR library, 22.5 μg psPAX2 and 7.5 μg pMD.2G. After 6 hours transfection, medium was replaced with 30 mL DMEM medium. The supernatant was collected, filtered, mixed with PEG8000 solution at 1:4 (v/v) ratio and concentrated lentivirus overnight. Lentiviral was centrifuged at 4500 rpm for 30 mins. Then, lentivirus was resuspended and stored at -80°C.

RBP CRISPR-cas9 screening

8.3×10^7 SW620 cells were transduced with concentrated RBP pooled CRISPR knockout library lentivirus (MOI=0.15) to achieve 1000 x library coverage and cultured with 10 mg/mL polybrene (Yeasen Biotechnology, 40804ES76) in 1640 medium for one day. Then, cells were treated with 2 mg/mL puromycin (ThermoFisher Scientific, A1113802). 1.3×10^7 SW620 cells were collected on day 5 (marked as day 0) and day 12 (marked as day 7) for each replicate.

Genomic DNA of day 0 and day 7 were extracted using MiniBEST Universal Genomic DNA Extraction Kit (Takara Biomedical Technology, #9765). For library construction, sgRNA sequences were amplified using Phanta Super-Fidelity DNA Polymerase (Vazyme, P501-d2) and one-step primers containing Illumina adaptors, lentiCRISPR v2 vector binding sequences and unique index sequence. PCR products were purified using FastPure Gel DNA Extraction Mini Kit (Vazyme, DC301-01) and sequenced using the Illumina NovaSeq 6000 platform. The sequencing results were calculated and identified using MaGeCK-v 0.5.9.5.⁴⁴

Immunohistochemistry (IHC) staining assay

11 CRC tumor and paired normal adjacent samples were fixed in 4% paraformaldehyde, dehydrated in ethanol and embedded with paraffin. Paraffin-embedded sample slices were deparaffinized, rehydrated and subjected to antigen retrieval. All slices were incubated with antibody against INTS3 (Proteintech, 16620-1-AP) overnight and secondary antibody for 1 h. Then, slices were stained with DAB working solution for 7 min and hematoxylin for 5 min. IHC images were acquired using a slide scanning system (Olympus VS200) and positive areas were calculated using ImageJ.

sgRNA, shRNA and overexpression cell lines

The sgRNA sequences (sgINTS3 #3, TGGGGATTATGGTCTCCAG; sgINTS3 #4, CTGTCCTGCAGTGATACGG) were obtained from RBP pooled CRISPR knockout library and cloned into TLCV2 (Addgene, # 87360). Lentivirus was generated by HEK293T and infected SW620. SW620-sgINTS3 cells and control cells were treated with 2 mg/mL puromycin (ThermoFisher Scientific, A1113802). INTS3 KO was induced by 1 μg/mL doxycycline (Solarbio Life Sciences, D8960).

All shRNA oligos (shINTS3 #1, GGATCTCGTAAGACTACTTCA; shINTS3 #2, GCAGAAAGTGTCTGGATATC; mshINTS3, GCTGC TACTTTCAACCAGTTT) were cloned into pSicoR-mCherry-empty (Addgene, # 21907). SW620, HCT116 and RKO were transduced with

pSicoR-mCherry-empty or pSicoR-mCherry-INTS3 vector. Mcherry positive cells were sorted by FACSymphony S6 system (BD Biosciences) for the downstream assays.

The CDS sequence of INTS3 was cloned in pLVX-puro vector. The pLVX-INTS3-puro vector or pLVX-puro vector was transfected into SW620. SW620-oeINTS3 and SW620-oeControl cells were treated with 2 mg/mL puromycin for the *in vitro* assays (ThermoFisher Scientific, A1113802).

Propagation/survival assay of human CRC cells

SW620-sgINTS3 #3, SW620-sgINTS3 #4 and SW620-sgControl cells were induced by DOX for 4 days and then were plated at 20,000 cells/well. 3-5 days after transduction, shINTS3 #1, shINTS3 #2 and shControl human colorectal cancer cells (50,000 SW620 cells/well, 20,000 HCT116 cells/well and 40,000 RKO cells/well) were plated. In this assay, CRC cells were counted daily up until 3-4 days and were stained with DAPI at the end-point of the experiment.

Annexin V-APC/7-AAD apoptosis assay

Apoptosis assays were performed using the Annexin V-APC/7-AAD Apoptosis Kit (Procell, P-CA-208). Briefly, cells were washed by cold PBS and were resuspended in 100 μ L and stained with 2.5 μ L Annexin-V-APC and 2.5 μ L 7-AAD. Then, cells were incubated in the dark for 15 min. 100 μ L binding buffer was added and analyzed using flow cytometry.

Cell proliferation assay

INTS3-LOF (loss of function) and control cells were seeded in 96-well plates. The cells were incubated with 10 μ M Edu (Beyotime, C0081S) for 2 h before fixation, permeabilization and click-it reaction. Then cells were stained with DAPI for 20 mins. Proliferating cells were scanned and analyzed by Thermo Scientific CX7LZR high-content analysis platform.

In vivo transplantation of human CRC cell lines

A total of 5×10^6 HCT116-shINTS3 cells (left flanks) or HCT116-shControl (right flanks) cells were injected into the back of male BALB/c nude mice. For RKO tumor cell mouse model, 8×10^6 RKO-shINTS3 #2 cells (left flanks) or RKO-shControl (right flanks) cells were injected. Tumor volumes were measured once every 2 days from the eighth day after injection. In Dox-inducible INTS3 knockout mouse model, a total of 5×10^6 SW620-sgINTS3 cells were injected into left back of the male BALB/c nude mice and 5×10^6 SW620-sgControl cells were injected into the right back.

Once the tumor volume reached 100 mm³, mice were treated with 2 mg/mL DOX drinking water to induce INTS3 knockout and tumors measured every other day. All tumor-bearing mice were sacrificed when tumor volumes reached 1000 mm³ and tumor weight was recorded. Tumor volume was calculated as follow: volume = $0.5 \times \text{length} \times \text{width}^2$.

mRNA sequencing

SW620-sgControl, SW620-sgINTS3 #3 and SW620-sgINTS3 #4 were isolated for total RNA. The RNA-seq was conducted by Berry Genomics (Fuzhou, China). Differential gene expression was analyzed and determined using $|\log_2 \text{fold-change}| > 1.6$ and $P\text{value} < 0.05$ (Results were shown in [Tables S1](#) and [S2](#)).

Nascent RNA labeling

Global transcription regulation was detected by labeling the nascent RNA. Cell-Light EU Apollo643 RNA Imaging Kit (RiboBio, C10316-2) was used to label nascent RNA. Briefly, cells were cultured in 500 μ M EU medium for 2 h and fixed with 4% paraformaldehyde/PBS for 30 mins at room temperature. Then EU-labeling cells were washed with 2 mg/mL glycine solution for 5 mins and permeabilized by 0.5% TritonX-100 for 10 mins. Finally, cells were cultured with click-it reaction buffer for 30 mins and detected by flow cytometry.

RNA stability assay

SW620-sgINTS3 #4 and control cells were treated with 5 μ g/mL ActinomycinD (Act D) (MedChemExpress, HY-17559). Cells were collected at 0, 1, 2, 4 and 8h to isolate total RNA and detected gene expression as described above. The half-life of RNA was calculated by its expression level at 1, 2, 4 and 8h relative to 0h. For the RNA-decay sequencing samples, cells were collected at 0, 2 and 4 hours (Results of RNA half-life were shown in [Table S3](#)).

RNA isolation, reverse transcription and RT-qPCR

VeZol reagent (Vazyme, R411-01) was used to extract total RNA. Total 1 μ g RNA was then reverse transcribed into complementary DNA (cDNA) using HiScript III RT SuperMix (Vazyme, R323-01). Real-Time Quantitative PCR (RT-qPCR) was carried out using AceQ Universal SYBR qPCR Master Mix (Vazyme, Q511-02). The primers of related genes can be found in [Table S4](#).

DOTAP/cholesterol liposome preparation and characterization

DOTAP and cholesterol (chol) were dissolved in chloroform and mixed (mol/mol=1:1) in a 100 mL-round-bottomed flask. Chloroform was removed by using rotary evaporation at 37°C water bath for 1 h. The obtained films were hydrated in 5% glucose water to a final concentration of 10 mM DOTAP/chol. DOTAP/chol liposome and mshINTS3 plasmid were mixed at different $\mu\text{g}:\mu\text{g}$ ratios (0:1, 1:1, 2:1, 3:1, 4:1, 5:1, 6:1, 10:1) to detect suitable package rate. Hydrodynamic size and zeta potential were detected by Malvern Instrument (Malvern, Nano ZS).

DOTAP/chol-mshINTS3 nanoparticle antitumor assay *in vivo*

To establish CRC tumor-bearing mouse model, male BALB/c mice were inoculated subcutaneously (s.c.) with CT26 cells (5×10^5) on the right flank. After one week, all mice were randomly in three groups and treated with 5% glucose water, plasmids of mshINTS3 or DOTAP/chol-mshINTS3 nanoparticles. Drugs were injected in tumor every 2 days for 7 times. The body weight of mouse and tumor volume (volume = $0.5 \times \text{length} \times \text{width}^2$) were record every other day. On the day 19, all mice were sacrificed and tumors were harvested and digested into single cells by using collagenase IV and Dnase I. Then, cells single cells were stimulated with 20 ng/mL PMA (Sigma), 1 μM ionomycin (Sigma) and protein transport inhibitor (555029, BD bioscience) for 4h. Cells were then labeled with anti-CD45-FITC (30-F11), anti-CD3-PerCP-eFluor710 (17A2), anti-CD8 α -BV605 (53-6.7) and anti-IFN- γ (XMG1.2) to analysis percentage CD8⁺ T cells and the interferon- γ (IFN- γ)-producing.

QUANTIFICATION AND STATISTICAL ANALYSIS

All data were analyzed using GraphPad Prism (GraphPad). ImageJ, a Java-based image processing program from the National Institutes of Health, was used for quantification of the IHC, tunel staining and colony formation data. Data are shown as mean \pm SD. Statistical significance was determined by t tests (two-tailed) for two groups and set at * $p < 0.05$, ** $p < 0.01$, *** $p < 0.001$.